Dissecting the proton transport pathway in electrogenic Na^+/H^+ antiporters

Povilas Uzdavinys[a,1], Mathieu Coinçon[a,1], Emmanuel Nji[a], Mama Ndi[a], Iven Winkelmann[a], Christoph von Ballmoos[b,2], and David Drew[a,2]

[a]Centre for Biomembrane Research, Department of Biochemistry and Biophysics, Stockholm University, SE-106 91 Stockholm, Sweden; and [b]Department of Chemistry and Biochemistry, University of Bern, CH-3012 Bern, Switzerland

Edited by Donald W. Hilgemann, University of Texas Southwestern Medical Center at Dallas, Dallas, TX, and accepted by Editorial Board Member David E. Clapham December 28, 2016 (received for review August 31, 2016)

Sodium/proton exchangers of the *SLC9* family mediate the transport of protons in exchange for sodium to help regulate intracellular pH, sodium levels, and cell volume. In electrogenic Na^+/H^+ antiporters, it has been assumed that two ion-binding aspartate residues transport the two protons that are later exchanged for one sodium ion. However, here we show that we can switch the antiport activity of the bacterial Na^+/H^+ antiporter NapA from being electrogenic to electroneutral by the mutation of a single lysine residue (K305). Electroneutral lysine mutants show similar ion affinities when driven by ΔpH, but no longer respond to either an electrochemical potential (Ψ) or could generate one when driven by ion gradients. We further show that the exchange activity of the human Na^+/H^+ exchanger NHA2 (*SLC9B2*) is electroneutral, despite harboring the two conserved aspartic acid residues found in NapA and other bacterial homologues. Consistently, the equivalent residue to K305 in human NHA2 has been replaced with arginine, which is a mutation that makes NapA electroneutral. We conclude that a transmembrane embedded lysine residue is essential for electrogenic transport in Na^+/H^+ antiporters.

secondary active transporters | proton transport | membrane protein | Na^+/H^+ exchangers | energetics

Sodium/proton antiporters are found in all cells, where they help to regulate intracellular pH, sodium levels, and cell volume (1). Na^+/H^+ antiporters are members of the large monovalent cation:proton antiporter (CPA) superfamily that includes, among others, the CPA1 and CPA2 clades (2). It is generally thought that Na^+/H^+ antiporters from the CPA1 clade catalyze electroneutral sodium–proton exchange (*SLC9A1-9*/NHE1-9, in mammals), whereas CPA2 members are thought to be electrogenic (*SLC9B1-2*/NHA1-2, in mammals) (2), with stoichiometries of $2H^+$:$1Na^+$ and $3H^+$:$2Na^+$ ions reported (3, 4). Their dysfunction is associated with a number of different diseases, and they are well-established drug targets (1, 2). In bacteria, Na^+/H^+ antiporters use the proton-motive force to extrude sodium out of the cell and, for this reason, are important classes of secondary active transporters for both bacterial homeostasis and pathogenesis (5).

Bacterial Na^+/H^+ antiporters harbor the "NhaA fold" (6, 7), which was first observed in *Escherichia coli* NhaA and has since been observed in an unrelated sodium-coupled bile acid symporter (8). The NhaA fold consists of a dimer domain and an ion translocation (core) domain, which is characterized by a six-helical bundle harboring two opposite-facing discontinuous helices that crossover near the center of the membrane. Although bidirectional proton (H^+) and sodium (Na^+) translocation is strictly coupled in antiporters, the underlying molecular mechanism is still not fully understood. It has been assumed that, for electrogenic Na^+/H^+ antiporters, two protons are carried across the membrane by two strictly conserved aspartate residues (2), which release their protons on the other side of the membrane in exchange for binding one sodium ion. Previous studies have shown that, for electrogenic transporters, both carboxyl-containing residues are essential (2, 9, 10), but, for electroneutral transporters, only one of the two aspartate residues is conserved (2). Despite this prevailing view, there is no direct measurement for proton transport by these aspartate residues per se, and this is not the only plausible mechanism. In the recent crystal structure of NapA, an electrogenic Na^+/H^+ antiporter from *Thermus thermophilus*, the two strictly conserved aspartate residues D157 and D156 are well positioned to bind protons; however, D156 was also found salt-bridged to a neighboring lysine residue, K305 (11). Likewise, in a new crystal form of dimeric *E. coli* NhaA at inactive pH, a salt bridge between the equivalent charged residues was also evident (12). The formation of the salt bridge between one of the conserved ion-binding aspartates suggests a different mechanism than direct protonation of the carboxylic residues, that is, one in which the lysine residue itself could be a proton carrier (12).

Previous studies have shown that the mutation of K305 in NapA to alanine (11, 13) or the equivalent lysine in *E. coli* NhaA to alanine, arginine, or histidine retains some antiport activity for Li^+ and the latter two also for Na^+ (10), but this activity has not yet been characterized in detail (10). In this study, we have analyzed the effect of pH to Na^+ and Li^+ catalyzed transport of NapA wild type (WT), mutants of K305, and other residues in the vicinity of the proposed ion binding site. Our data support a transport model in which protons and $Na^+(Li^+)$ compete

Significance

Cells express transporters that strictly exchange protons for sodium ions to regulate many fundamental processes, such as intracellular pH and cell volume. The bacterial Na^+/H^+ exchangers typically use the energy stored in membrane potentials, whereas the mammalian transporters do not. The energetic difference stems from the ability of the bacterial proteins to transport multiple protons in exchange for one sodium ion. The mechanism for how this is achieved, however, has remained elusive. Here, using purified components in synthetic membranes, we have compared the energetics and kinetics of the bacterial exchanger NapA to the human exchanger NHA2, which has been linked to insulin secretion. Remarkably, the judicial placement of a transmembrane embedded lysine is the key for harnessing a membrane potential.

Author contributions: C.v.B. and D.D. designed research; P.U., M.C., E.N., M.N., and I.W. performed research; C.v.B. contributed new reagents/analytic tools; P.U., M.C., E.N., M.N., I.W., C.v.B., and D.D. analyzed data; and C.v.B. and D.D. wrote the paper.

The authors declare no conflict of interest.

This article is a PNAS Direct Submission. D.W.H. is a Guest Editor invited by the Editorial Board.

[1]P.U. and M.C. contributed equally to this work.

[2]To whom correspondence may be addressed. Email: david.drew@dbb.su.se or christoph.vonballmoos@dcb.unibe.ch.

This article contains supporting information online at www.pnas.org/lookup/suppl/doi:10.1073/pnas.1614521114/-/DCSupplemental.

for the same ion binding site. Although most K305 mutations in NapA are functional, only the substitution with histidine can generate a membrane potential, revealing the essential role of K305 as a proton carrier and for conferring electrogenicity. We further show that these findings are consistent with the electroneutral antiport activity measurements of the purified human Na^+/H^+ exchanger NHA2, a protein that harbors the same strictly conserved aspartate residues, but where the residue equivalent to K305 has been replaced by arginine.

Results

pH-Dependent Activity Is an Intrinsic Property of the Ion Binding Site. Using solid-supported membrane electrophysiology, it was shown that the strongly pH-dependent activity for the homologous antiporter *E. coli* NhaA can be fitted by a simple kinetic model in which Na^+ and protons compete for the same ion binding site (14). At acidic pH values, the K_m for Na^+ is strongly affected by competition of the elevated proton concentration to the same binding site, whereas V_{max} of the transporter is unaltered. At alkaline pH, however, where affinity for Na^+ is high because of the low proton concentration, activity is dictated by an altered V_{max}. Together with other biochemical data (14), these results strongly suggested that pH regulation is an intrinsic property of the ion binding site and not a separate step in the transport cycle, as was originally proposed (1, 15).

Although, in NhaA, both Na^+- and Li^+-driven activity show a clear pH dependence profile, the activity for NapA was reported to be atypical in that its activity was shown to be pH-dependent for Na^+, but not for Li^+ over the physiological pH ranges tested (13). The simplest interpretation is that the different pH activity profiles reflect the 10-fold lower apparent affinities for Na^+ compared with Li^+ (11, 13, 16). As such, in NapA, protons could be more effective at competing for the binding of Na^+ than for Li^+. To test this hypothesis, purified NapA was coreconstituted together with *E. coli* F_0F_1 ATP synthase into liposomes (*Materials and Methods* and Fig. 1*A*). In these liposomes, F_0F_1 ATP synthase has an inside-side-out orientation, whereas, based on maleimide-PEG-5k labeling efficiency to a cytoplasmic located cysteine mutant V31C, NapA has a ∼60 to 70% right-side-out orientation (Fig. S1*A*), i.e., preference is toward the physiological orientation. In these experiments, the ATP synthase acidifies the inner volume of the liposomes by ATP-driven proton pumping, which is monitored by a decrease in the fluorescence of the ΔpH-sensitive dye 9-amino-6-chloro-2-methoxyacridine (ACMA). Addition of Na^+ or Li^+ ions at various concentrations drives proton efflux by NapA, which is seen as an increase in ACMA fluorescence (dequenching) (Fig. 1*B*). Based on the amount of ACMA dequenching over a range of different ion concentrations, an apparent K_m can be determined (17) (*Materials and Methods*). In these experiments, potassium and valinomycin are always present in the proteoliposomes to stop the buildup of a membrane potential (ΔΨ); transport is primarily driven by the outwardly directed pH gradient.

The amount of ACMA dequenching upon the addition of 5 mM Li^+ or Na^+ to NapA proteoliposomes acidified by ATP synthase was measured from pH of 6 to 8.5 (Fig. 1*C*). The apparent affinities (K_m) for Na^+ and Li^+ were also determined at each external pH (Fig. 1*C*, numbers next to data points). Although the apparent K_m for Li^+ increases only sevenfold from pH 8.5 to 6 (0.5 mM to 3.5 mM), the K_m for Na^+ was much more pH-sensitive, increasing >50-fold from pH 8.5 to 6 (0.7 mM to 38 mM). At pH 8.5, the apparent K_m of NapA for Li^+ and Na^+ ions and the amount of ACMA dequenching observed at 5 mM were nearly equivalent.

Based on the above reasoning, weakening the ion binding site by point mutations should result in Li^+-driven activity that is now pH-dependent over the physiologically relevant pH ranges tested. To explore this rationale, potential ion binding

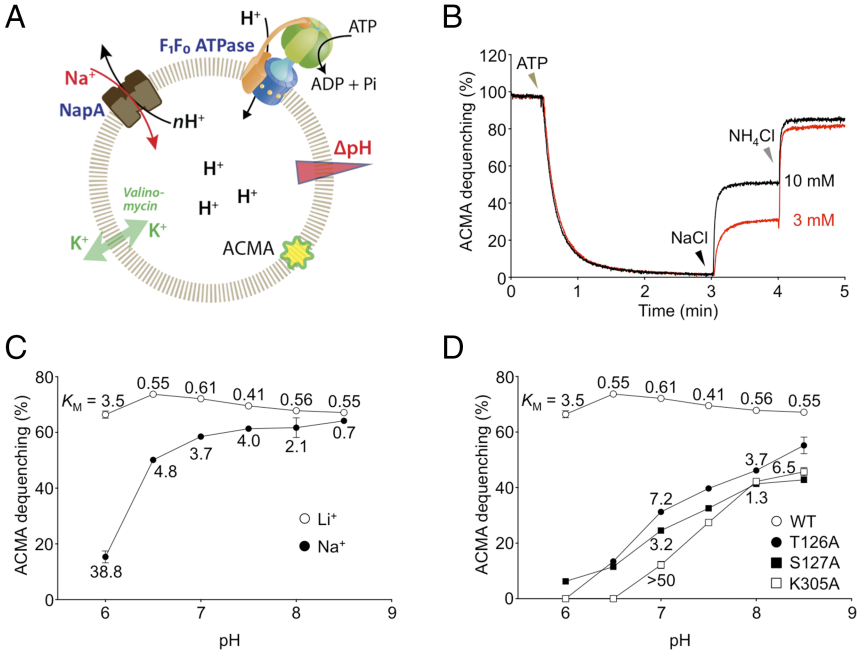

Fig. 1. The pH dependence of NapA and its putative ion binding site. (*A*) Cartoon showing the experimental setup for determination of Na^+/Li^+ affinity. The ATP synthase and NapA are coreconstituted into liposomes. Free K^+ diffusion by valinomycin suppresses the effect of ΔΨ. ACMA, 9-amino-6-chloro-2-methoxyacridine. (*B*) Representative ACMA fluorescence traces for Na^+/H^+ antiporter activity. ATP-driven H^+ pumping (brown arrow) establishes a ΔpH (acidic inside) as monitored by quenching of fluorescence. H^+ efflux is initiated by the addition of NaCl/LiCl (black arrow), and further NH_4Cl addition (gray arrow) collapses the proton gradient. (*C*) The pH dependence of Na^+/H^+ (5 mM) and Li^+/H^+ (5 mM) antiport activities of NapA WT. Apparent affinity values (K_m) are shown at certain pH values. (*D*) Comparison of Li^+/H^+ antiport activities of NapA WT (5 mM) and mutants (10 mM) with apparent K_m values at certain pH values.

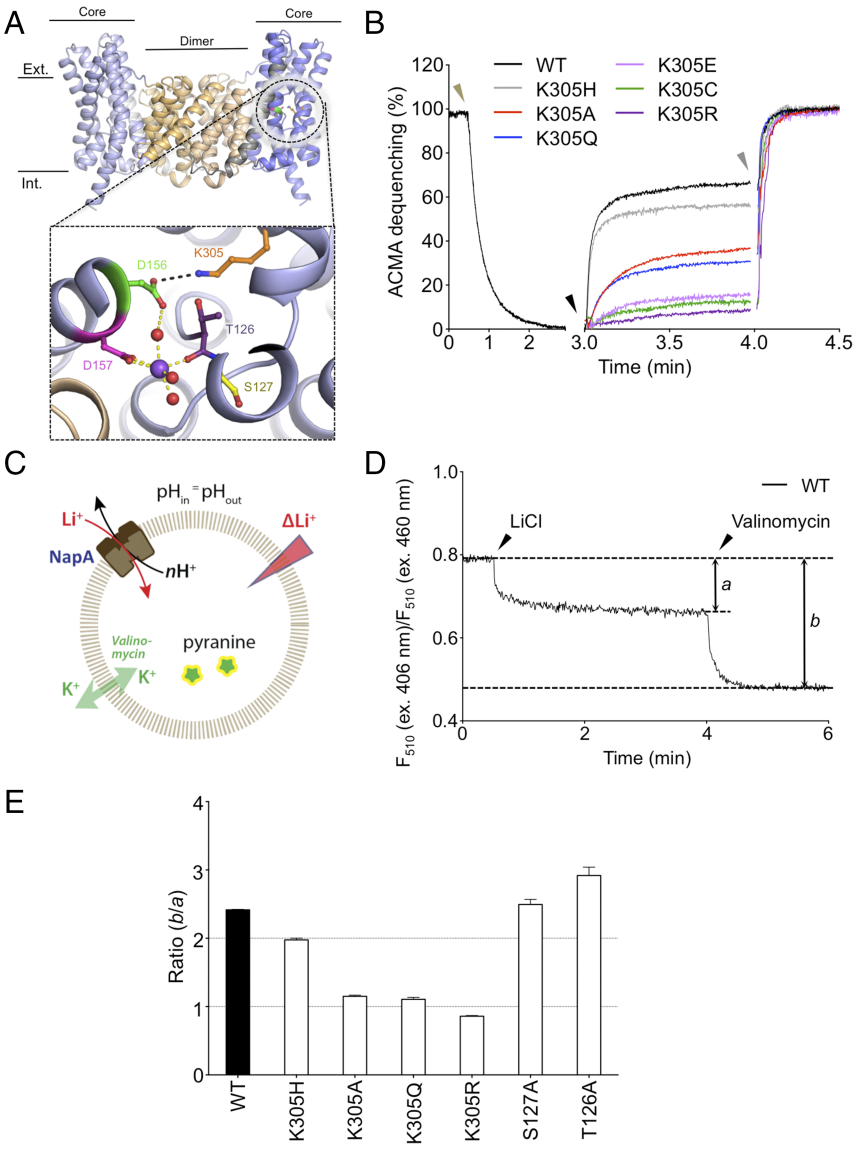

Fig. 2. Switching NapA WT activity from being electrogenic to electroneutral. (*A*) Cartoon representation of dimeric NapA. Ion translocation domain (core) is colored in blue, dimerization domain (dimer) in wheat, and the linker transmembrane helix (TM6) in gray. Residues used for mutagenesis are depicted in stick form in the right protomer and color-coded (S127 yellow, T126 purple, D156 green, D157 magenta and K305 orange). (*Inset*) The ion binding site extracted from an Na^+ (purple sphere) bound state of a molecular dynamic simulation (16). The salt bridge between K305 and D156 is depicted by black dashed line. Water molecules coordinating the ion are represented by red spheres. (*B*) Representative ACMA fluorescence traces for NapA WT and its mutants at pH 8.0 for Li^+/H^+ antiport activity (20 mM). Brown arrow, addition point of ATP (120 μM); black arrow, addition point of LiCl (20 mM); gray arrow, addition point of NH_4Cl (20 mM). (*C*) Cartoon showing the experimental setup for Li^+-driven proton efflux experiments. In the starting conditions, pH values on the inside and outside are identical. Lithium addition drives H^+ efflux, and alkalinization of the liposome volume is monitored by the pH-sensitive dye pyranine. Valinomycin is added to extinguish the membrane potential. (*D*) NapA activity monitored with liposome-entrapped pH-sensitive fluorophore dye pyranine recorded at 510 nm (excitation 406 and 460 nm). In WT NapA, addition of LiCl (40 mM) at pH 8.0 builds up a membrane potential (distance a) that was dissipated upon addition of valinomycin at 4 min (distance b) and leads to further H^+ efflux; this releases the inhibitory membrane potential established during the first transport phase. (*E*) Valinomycin sensitivity for NapA WT and mutants was calculated by measuring the ratio between distance b and distance a; see *D*.

site residues T126 and S127 (Fig. 1*D* and Fig. 2*A*) were substituted with alanine; mutants of the conserved aspartates D156 and D157 cannot be directly assessed, as they are completely nonfunctional (11, 13). A weakening of the binding affinity was indeed observed, as the T126A mutation caused a sixfold increase in the apparent K_m for Li^+ from 0.5 to 3.7 mM at pH 8 (Table 1). As predicted, activity for T126A was now also strongly pH-dependent for Li^+, with no detectable activity at pH 6 (Fig. 1*D*). The same pattern, but less pronounced, is also observed for S127A (Fig. 1*D*). This weaker effect could be because the side-chain of S127 is more distal to the predicted ion binding site than the side-chain of T126 (Fig. 2*A*). Finally, a third mutation, K305A, was investigated and displayed similar behavior, supporting our idea that K305 affects the ion binding properties in NapA (Table 1). Taken together, the results show that the pH-dependent activity of NapA is an intrinsic property of the ion binding site.

Converting Electrogenic NapA into an Electroneutral Transporter. Recently, an outward-facing crystal structure of NapA was determined at active pH 6.5 and refined at 2.3 Å resolution (16).

Table 1. K_m values in mM of WT NapA and human NHA2 and studied mutants from pH 6.0 to 8.0

NapA	pH 6.0		pH 6.5		pH 7.0		pH 7.5		pH 8.0	
	Na^+, mM	Li^+, mM	Na^+, mM	Li^+, mM	Na^+, mM	Li^+, mM	Na^+, mM	Li^+, mM	Na^+, mM	Li^+, mM
WT	38.8 ± 5.4	3.5 ± 0.2	4.8 ± 0.2	0.55 ± 0.03	3.7 ± 0.2	0.61 ± 0.04	4.0 ± 0.3	0.41 ± 0.04	2.1 ± 0.1	0.56 ± 0.02
K305A	—	—	—	—	—	>50	—	—	—	6.5 ± 0.5
K305H	34.1 ± 9.3	3.5 ± 0.2	5.2 ± 0.3	0.51 ± 0.02	3.5 ± 0.2	0.52 ± 0.04	—	—	2.0 ± 0.1	0.63 ± 0.03
K305Q	—	—	—	—	—	—	—	—	11.9 ± 1.2	1.7 ± 0.2
K305R	—	—	—	—	—	—	—	—	—	>75
K305E	—	—	—	—	—	—	—	—	—	20.4 ± 5.0
K305C	—	—	—	—	—	—	—	—	—	24.8 ± 3.1
S127A	—	—	—	—	—	3.2 ± 0.4	—	—	>75	1.3 ± 0.07
T126A	—	—	—	—	—	7.2 ± 0.3	—	—	>75	3.7 ± 0.2
D156N K305Q	—	—	—	—	—	—	—	—	>75	>75
hsNHA2 WT	—	—	—	—	—	—	—	—	67.5 ± 12.7	32.8 ± 7.6
hsNHA2 R362K	—	—	—	—	—	—	—	—	>75	>75
hsNHA2 R362H	—	—	—	—	—	—	—	—	>75	>75

The apparent K_m for K305R mutant are 34.7 ± 4.7 mM and 84.7 ± 17.2 mM for LiCl, at pH 8.5 and pH 9.0, respectively.

However, it was still not possible to unambiguously identify a bound Na^+ ion in the electron density maps at the proposed ion binding site (16). Molecular dynamics (MD) simulations of the NapA crystal structure were therefore performed to investigate potential Na^+ ion coordination (16). Similar to the binding mode seen in MD simulations of *E. coli* NhaA (11, 16), conserved aspartic acids D157 and D156 as well as T126 were seen to coordinate Na^+ in the middle of the discontinuous helix crossover (Fig. 2*A*, *Lower*). However, unlike NhaA, where Na^+ binding in MD simulations was also seen to favor breakage of the salt bridge between D163 and K300 residues (12), in NapA, the equivalent salt bridge between K305 and D156 residues always remained intact, even upon Na^+ binding (16). This discrepancy may reflect the parameters used to model ion binding in the MD simulations or structural differences between the two proteins. Regardless, it highlights that experimental data are essential before any firm conclusions can be made regarding the potential role of K305 as a proton carrier. Hence, we forthwith substituted K305 to neutral and negatively and positively charged residues and determined the K_m of the purified mutants in our proteoliposome-based transport setup.

Only the substitution of K305 to histidine was able to support WT Na^+-driven transport activity (Table 1). The K305H variant also showed a pH-dependent activity indistinguishable from that of WT NapA (Fig. S1*B*). Overall, apart from the K305Q mutant that showed a fivefold higher K_m for Na^+, all other lysine variants were almost completely inactive for Na^+ up to ∼300 mM. All K305 variants do, however, retain some Li^+-driven transport activity (Fig. 2*B*), where K305H and K305Q were the least perturbing variants, with K_m values for Li^+ equal to and threefold higher than WT, respectively (Table 1). Surprisingly, the variant with the poorest Li^+-driven transport activity was the substitution of K305 to arginine with a K_m greater than 50 mM at pH 8. The apparent K_m dropped slightly to ∼35 mM at pH 8.5, but was again higher at pH 9 (>80 mM). At these higher pH values, Na^+-driven activity for the K305R variant was likewise immeasurable up to ∼300 mM (Table 1). Thus, a positively charged residue is, in of itself, insufficient to retain robust transport activity in this position. Other lysine variants K305A, K305E, and K305C had K_m values that were between 10- and 60-fold higher than WT (Fig. 2*B* and Table 1).

Because NapA is electrogenic (two protons are exchanged for one $Na^+(Li^+)$ ion), every ion gradient-driven turnover builds up a membrane potential that opposes, and eventually inhibits, proton transport. If the membrane potential is dissipated by the addition of valinomycin (in the presence of potassium), ion-driven transport is no longer hindered, and a new steady-state level can be reached (11). In contrast, the addition of valinomycin should not increase the transport activity in electroneutral Na^+/H^+ antiporters, as there is no membrane potential generated to oppose proton transport. We exploited this behavior to analyze the electrogenicity of the measurable Li^+ transport activity in the K305 variants. To this end, NapA WT and ion-binding variants were reconstituted into proteoliposomes in the presence of the water-soluble pH ratiometric dye pyranine, but in the absence of Li^+ (Fig. 2*C*). As shown for WT NapA, after the addition of Li^+, the fluorescence signal rapidly reached a first steady-state level (Fig. 2*D*). Upon the subsequent addition of valinomycin, the membrane potential was dissipated, and a second, final steady-state level was reached. Transport activity before and after valinomycin addition showed an approximately twofold to threefold ratio increase for WT NapA (Fig. 2 *D* and *E*), which is similar to that previously observed for *E. coli* NhaA (18). For the ion-binding variants S127A and T126A, the relative ratio increase in activity after the addition of valinomycin was also similar to that observed for WT (Fig. 2*E* and Fig. S1*C*). For the lysine variants K305A and K305Q, however, no obvious increase in exchange activity was observed with a ratio close to 1 (Fig. 2*E*). The difference is unlikely due to the poor activity of the K305A and K305Q variants, because they showed similar K_m values for Li^+ as the valinomycin-sensitive variants T126A and S127A (Table 1). Indeed, with the exception of K305H, all lysine variants including K305R no longer responded to valinomycin (Fig. 2*E* and Fig. S1*C*).

As WT NapA is electrogenic, we have recently shown that Na^+/H^+ exchange can be efficiently driven solely by a membrane potential ($\Delta\Psi$) in the absence of proton and sodium gradients (11). If all of the K305 variants, except for histidine, are indeed electroneutral, it should not be possible to drive their activity under these conditions. To test this hypothesis, WT NapA and all of the ion binding site variants were reconstituted into pyranine-encapsulated liposomes containing 100 mM KCl and 100 mM Li^+ at pH 7.8 and suspended into the same buffer composition, but with only 1 mM KCl (Fig. 3*A*). With no ion gradients present, the only driving force applied was an electrical potential of ∼116 mV (inside negative), which is generated when valinomycin was added to the proteoliposomes (Fig. 3*B*). As shown in Fig. 3*B*, WT NapA, T126A, S127A, and K305H variants all showed strong $\Delta\Psi$-driven activity. In contrast, all of the K305 variants, which were previously shown to be valinomycin-insensitive, showed little or no $\Delta\Psi$-driven transport activity (Fig. 3*B*). We further assessed the dependence of antiporter activity on the electrical potential in the range from −5 to −116 mV, as shown in Fig. S1*D*. Again, only WT NapA and the K305H, T126A, and

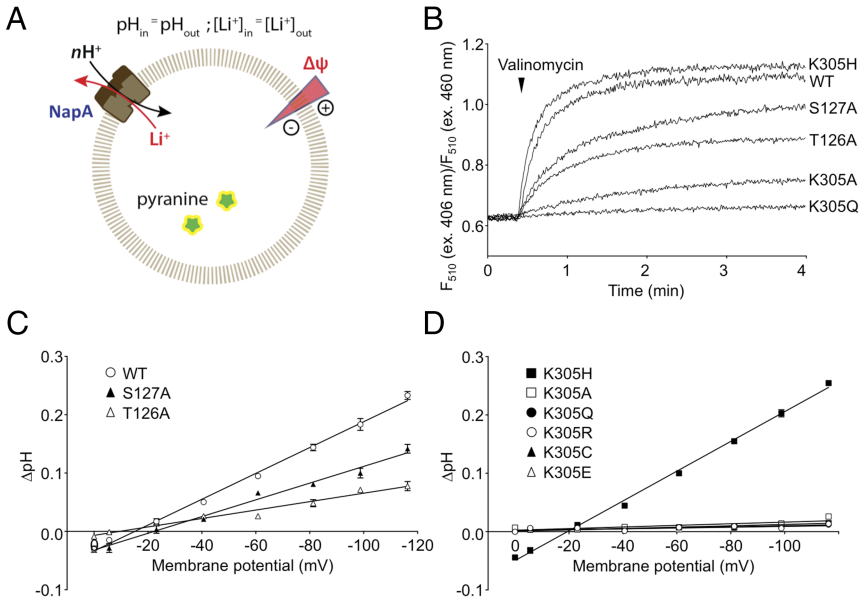

Fig. 3. NapA WT and mutant antiport activity when driven by a membrane potential. (*A*) Cartoon showing the experimental setup for $\Delta\Psi$-driven proton influx experiments. In the starting conditions, H^+ (pH 7.8) and Li^+ (100 mM) concentrations are identical. Addition of valinomycin generates a Nernst potential (negative inside) that energizes proton influx in electrogenic transporters that is monitored by the entrapped pyranine. (*B*) Pyranine traces depicting the amount of WT NapA and mutant activity when transport was driven solely by an electrical potential of −116 mV. (*C* and *D*) NapA WT and mutants' response to increasing membrane potentials (Ψ), which was established by a K^+-diffusion potential, using different KCl concentrations in the measuring buffer.

S127A variants showed a linear increase in activity with increasing voltages (Fig. 3 *C* and *D* and Fig. S1 *E* and *F*), while the electroneutral variants showed no voltage-dependent increase in activity (Fig. 3*D* and Fig. S1 *E* and *F*).

The absence of a stimulating effect after dissipation of $\Delta\Psi$ in all of the K305 variants except for histidine, together with their inability to be driven solely by an electrical potential, suggests that the K305 residue is essential for electrogenic transport. Consequently, these mutants should not generate a membrane potential when driven by ion gradients. To confirm this, we used the fluorescent dye 3,3′-dipropythiadicarbocyanine iodide [$DiSC_3(5)$], because it is sensitive to an electrical membrane potential (negative inside) and has been previously used to show electrogenic transport of *E. coli* NhaA (19). In these experiments, either NapA WT or K305 variants were reconstituted into liposomes and the $DiSC_3(5)$ dye added (Fig. 4*A*). Upon addition of Na^+ or Li^+, an uneven $Na^+(Li^+)/H^+$ stoichiometry, as found in WT NapA, quickly generated a membrane potential, which was observed by a decrease in $DiSC_3(5)$ fluorescence (Fig. 4*B*, black trace). In the presence of potassium, the membrane potential was abolished by valinomycin and the signal returned close to the starting level (Fig. 4*B*); to establish a background signal, proteoliposomes containing either no protein or the inactive variant D157N were used (Fig. 4*B*, green and orange traces). Next, we tested the variants S127A and K305H, which showed electrogenic activity in the previous experiments. As shown in Fig. 4*C*, upon the addition of lithium, these variants generated a membrane potential, wherein S127A showed a weaker response than either K305H or WT. In contrast, variants K305A, K305Q, and K305R showed no membrane potential generation, as their responses were indistinguishable from the background levels of the negative controls (Fig. 4*D*). These data are thus in complete agreement with the other two assays, reinforcing the view that the pumping stoichiometry in K305 mutants has been altered and is now close, or equal, to 1:1. The only exception, again, was K305H, which, remarkably, appeared to generate an electrical potential similar to that observed for NapA WT (Fig. 4*C*).

Low Internal pH Facilitates Ion Exchange Activity in NapA. In NapA WT proteoliposomes encapsulated with pyranine, a very strong change in fluorescence was observed upon the addition of Li^+ at pH 8 (Fig. 2*D*). In contrast, the addition of Li^+ to the electroneutral K305 variants showed a much smaller response (Fig. S1*C*). The difference in the Li^+-driven response could not be simply explained by a difference in activities, because, in the ΔpH-driven ACMA experiments, the apparent ion affinities of a number of the electroneutral and electrogenic mutants were determined to be similar, for example, S127A and K305Q (Table 1). The main difference between the two proteoliposome setups is that, in the ΔpH-driven experiments, ATP synthase pumps protons into liposomes until the internal pH becomes quite acidic (<pH 6), whereas, in the pyranine containing liposomes, the pH is ∼8 on both sides of the membrane, i.e., in absence of the ATP synthase, a proton gradient is not present during the pyranine experiments, and transport is driven solely by the applied Li^+ gradient. We reasoned that perhaps a low internal pH might facilitate exchange activity by increasing the likelihood of protonating key ion-binding residues, which would promote intracellular Li^+ release in a simple competition mechanism. To test this hypothesis, NapA WT and K305 variants in pyranine-encapsulated proteoliposomes were prepared, and the pH was adjusted to 6.6, 7.3, or 8.0 (Fig. 5*A*). Subsequently, proteoliposomes were diluted into buffer at each of the respective pHs, and Li^+-driven proton efflux was followed as described above. At pH 8, transport in the K305A and K305Q variants is quickly exhausted and does not even reach the first steady-state level seen in WT NapA (Fig. 5*A*). At pH 7.3, however, K305A and K305Q variants still perform similarly, but somewhat better compared with WT. At this pH, it is also seen that the transport process is now clearly slower in the NapA variants. Most interestingly, at pH 6.6, K305Q clearly performs better than K305A and almost reaches the first steady-state level of WT. Variant T126A also showed a pH-dependent decrease of the initial rate; however, the sensitivity toward $\Delta\Psi$ is seen at all pH values. The observed effects reinforce that K305 is at the core of the transport mechanism.

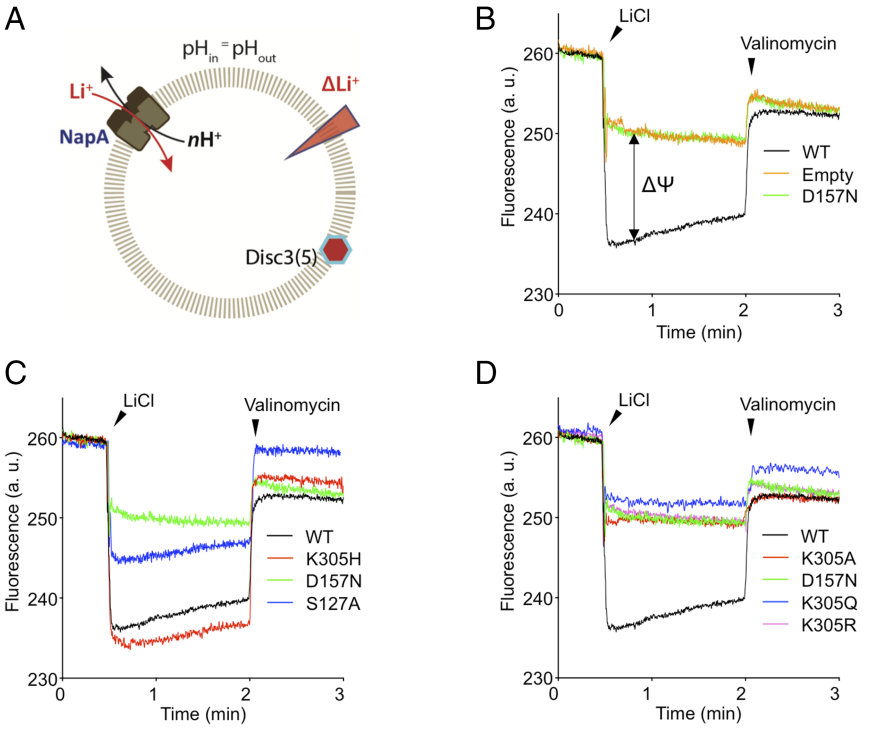

Fig. 4. Membrane potential generation in NapA WT and mutants. (*A*) Cartoon showing the experimental setup for Li^+-driven proton efflux experiments. In the starting conditions, pH values on the inside and outside are identical. Lithium addition drives H^+ efflux, and if a membrane potential is generated it was detected by the potential-sensitive dye $DiSC_3(5)$. (*B*) $DiSC_3(5)$ fluorescence traces showing the generation of a membrane potential in NapA WT (black trace). Valinomycin is added to extinguish the membrane potential. Negative controls with either empty liposomes or liposomes containing D157N are also shown. (*C*) Similar to *B*, but electrogenic variants K305H and S127A are shown. (*D*) Similar to *B*, but electroneutral variants K305A, K305Q, and K305R are shown.

An Interaction Between D156 and K305 Residues Is Central for Transport. In addition to the role of K305 as a proton carrier, MD simulations have also indicated that the salt bridge formed between corresponding residues in NhaA is sensitive to ion binding (12, 20). We therefore speculated that perhaps the reason why mutations of the equivalent D156 aspartate in NapA homologues are always inactive (1, 10, 11, 13) may not necessarily be because the variants are incapable of $Na^+(Li^+)$ binding but because such a mutation generates an "unpaired" lysine. To probe the importance of this interaction, we combined the nonfunctional D156N mutant with a K305Q variant, which was the least perturbing of the neutral lysine variants tested (Table 1). Strikingly, the D156N-K305Q mutant now showed robust ΔpH-driven antiport activity with ∼40% ACMA dequenching for both Li^+ and Na^+ ions at high ion concentrations (Fig. 5*B*). Although the apparent K_m for Li^+ and Na^+ are higher than WT (Table 1), this nonetheless demonstrated that, mechanistically, the second aspartate is not essential for ion-coupled transport, which is consistent with its replacement to asparagine in electroneutral Na^+/H^+ exchangers (2). As expected, the activity for the D156N–K305Q double mutant is also electroneutral, as no increase in antiport activity after valinomycin addition was observed (Fig. 5*C*).

Human NHA2 Antiport Activity Is Likely Electroneutral. In recent years, human Na^+/H^+ exchangers NHA1 and NHA2 have been described, with the latter proposed to have a role in hypertension and insulin secretion (21–23). Compared with the human cation exchangers NHE1-9, NHA1 and NHA2 have higher sequence similarity to the bacterial homologues, especially NapA (21% protein sequence identity). NHA2 (*SLC9B2*) also appears to be the only mammalian Na^+/H^+ exchanger where both aspartic acid residues equivalent to D156 and D157 are conserved (Fig. S2). However, unlike NapA, the residue equivalent to K305 is an arginine (Fig. S2). Furthermore, in contrast to the NHEs that use the inwardly directed Na^+ gradient to extrude protons, NHA2 is thought to be similar to (most) bacteria that use the proton gradient/membrane potential to extrude sodium (24). Consistent with this idea, NHA2 is found to localize to late endosomes, where it further colocalizes with the vacuolar ATPase (V-ATPase) (25), which establishes a low pH on the inside of endosomes. Because of the two conserved aspartates and the similarity to the bacterial homologues, NHA2 was thought to be electrogenic, but experiments in whole cells have not supported this assumption (2, 22–24, 26). We therefore aimed to clarify the energetics of human NHA2 in an isolated system using purified components.

First, an N-terminal tail Δ71 amino acid truncation mutant of human NHA2 was produced using fluorescent-based screening methods in *Saccharomyces cerevisiae* (27, 28) and purified in the detergent dodecyl-β-D-maltopyranoside (DDM) (*Materials and Methods* and Fig. S3*A*). Next, together with ATP synthase from *E. coli*, hNHA2 was coreconstituted into liposomes made from a mixture of brain and soybean lipids, which consistently gave the highest activity out of the various combinations of lipids tested (*Materials and Methods*). Using the same antiport assay as for NapA, we were able to obtain robust transport activity for hNHA2 after the addition of either Li^+ or Na^+ ions (Fig. 6*A*). Similar to *E. coli* NhaA (29), steep pH-dependent sensitivity for both Na^+ and Li^+ ions was observed between pH 6.5 and 8.5, with a maximal activity at pH 8.5 (Fig. 6*B*). The apparent affinities (K_m) for Li^+ and Na^+ were determined at pH 8.0 to be in a physiological range, ∼33 and 67 mM, respectively (Fig. S3*B*).

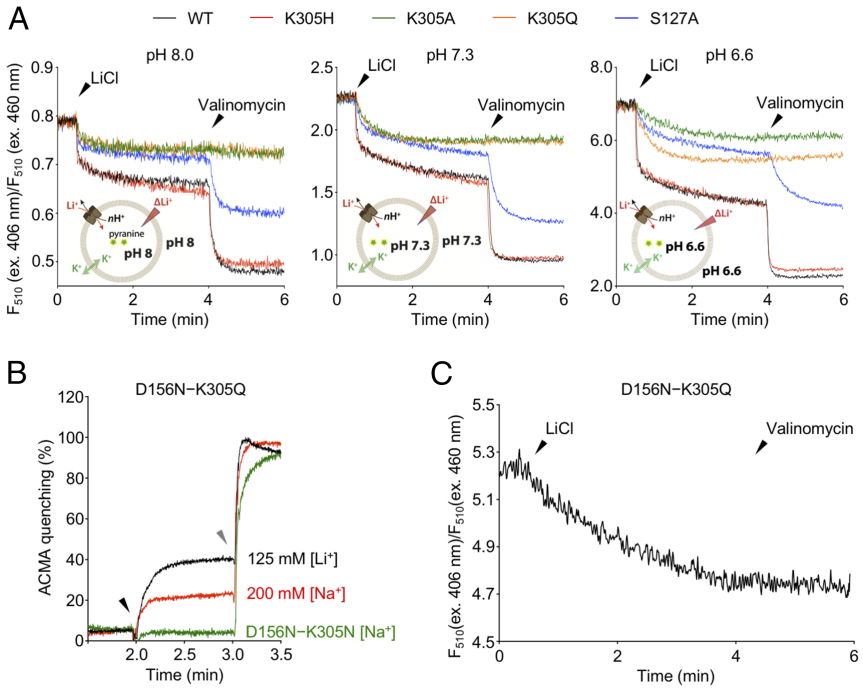

Fig. 5. ΔLi^+-driven proton efflux of NapA WT and mutants at different pH values. (*A*) In the absence of ΔpH, upon the addition of substrate generating an Li^+ concentration gradient (30 mM), WT NapA and mutants are more active at pH 6.6 and less active at pH 8.0; ΔH^+ was calculated as described in *Materials and Methods*. (*B*) Representative AMCA traces for Li^+ (black) and Na^+ (red) showing that an inactive D156N mutant was rescued by the additional mutation of K305 to glutamine; K_m = 106 ± 22 mM for Li^+ and K_m = 360 ± 112 mM for Na^+. In contrast, activity of the D156N mutant could not be rescued by the additional mutation K305N [green traces (Na^+)]; black arrow, addition of LiCl or NaCl; gray arrow, addition of NH_4Cl (20 mM). (*C*) As described in Fig. 2*D*, the valinomycin sensitivity of the NapA D156N-D305Q mutant was measured upon addition of Li^+ (pH 6.6).

To test if Li^+ catalyzed activity of hNHA2 is electrogenic, it was forthwith reconstituted into proteoliposomes in the presence of pyranine, as shown previously for NapA. Although the signal for Li^+ catalyzed proton efflux was small, a consistent difference compared with the nonfunctional ion-binding aspartate variant D279N was observed (Fig. 6*C* and Fig. S3*C*). Under these conditions, the addition of valinomycin, however, showed either a small or no clear increase in hNHA2 antiport activity at either pH 7.3 or 6.6, respectively (Fig. 6*C* and Fig. S3*D*). To clarify this ambiguous response to valinomycin, we assessed the dependence of NHA2 antiporter activity in the presence of a −116-mV potassium diffusion potential (Fig. 6*D*). However, no $\Delta\Psi$-driven proton influx could be observed for hNHA2 with traces indistinguishable from that observed for empty liposomes.

Discussion

Recently, we reported crystal structures of NapA in both outward- and inward-facing conformations (16). By comparing these two structures, we could show that alternating access to the ion binding site is likely achieved through large, elevator-like rearrangements of the core ion translocation domain. To begin to establish how ion binding and transport is coupled to these structural rearrangements, it is essential to dissect the residues required to drive electrogenic activity. Although a thallium-bound structure of the homologous protein NhaP from *Pyrococcuss albicans* has provided some insight into how Na^+ may bind (30), because NhaP is electroneutral, it provides little insight into the mechanism required to establish proton transport in electrogenic Na^+/H^+ antiporters.

Here, we have probed the role of the highly conserved transmembrane embedded lysine residue K305, which was implicated recently as a potential proton carrier, because of its salt-bridge formation, to one of the strictly conserved ion-binding aspartates in both NapA and NhaA crystal structures (11, 12, 16). Poignantly, the K305 residue is also positioned in the same location as the $Na(2)^+$ ion in sodium-driven bile acid symporters, which are structural homologues of Na^+/H^+ exchangers (8, 31). Our results clearly show that, apart from a K305 to histidine variant, which retains WT behavior, all other variants tested lost their ability for activity (*i*) to be stimulated by the dissipation of the membrane potential, (*ii*) to be driven with an electrical gradient alone, and (*iii*) to generate an electrical potential when driven by ion gradients. Thus, we were able to switch the activity of NapA from being electrogenic to electroneutral by the mutation of lysine K305 to any of the amino acids tested, except for histidine. The exceptional ability of histidine to retain WT activity supports these conclusions, as it is the only amino acid replacement that can still change its protonation state within a physiological pH range of ∼4 to 9. In contrast, a K305R variant shows no clear activity even at pH 9, presumably because the pK_a of arginine is too high and will predominantly be protonated over this pH range (Table 1). Interestingly, the apparent K_m values and the kinetic traces for the K305H are indistinguishable from WT, and, in this regard, it is somewhat surprising that this mutation, as far as we can ascertain, has never been acquired during evolution.

In light of our data, this means that, almost certainly, the residues equivalent to D157 and K305 are the two dominant proton carriers in all homologous electrogenic Na^+/H^+ antiporters. However, if D156 is not a proton carrier, why is this residue so essential for activity in electrogenic antiporters (1, 2)? Because D156 is not conserved in electroneutral antiporters, we hypothesized that its role in electrogenic antiporters, rather than strictly for ion coordination, is also to interact with K305, providing the required molecular environment for electrogenic antiport. To evaluate the importance of the D156 and K305 interaction, we simultaneously replaced D156 and K305 residues with uncharged polar residues and showed, for the first time, that

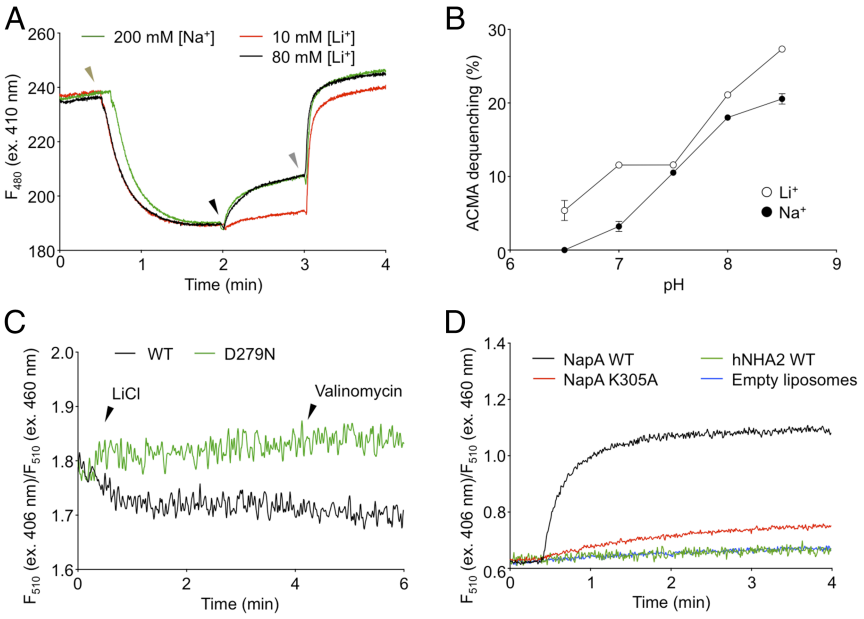

Fig. 6. The energetics of human NHA2 (hNHA2) antiport activity. (*A*) Representative ACMA fluorescence traces for hNHA2 antiport activity using the setup described for NapA in the legend of Fig. 1*A*. (*B*) The pH-dependent sodium (150 mM) and lithium (60 mM) activity for hNHA2. (*C*) The hNHA2 activity was monitored with liposome-entrapped pH-sensitive fluorophore dye pyranine recorded at 510 nm (excitation 406 and 460 nm). In hNHA2, addition of LiCl (60 mM) at pH 7.3 does not seem to build up a membrane potential, as no additional increase in H^+ efflux was observed following addition of valinomycin at 4 min (black trace). As a comparison, the inactive aspartate mutant D279N is shown (green trace). (*D*) The dependency of hNHA2 antiporter activity in the presence of a −116 mV potassium diffusion potential, displaying an absence of $\Delta\Psi$-driven proton influx. The pyranine traces depicting the relative activities are shown for WT NapA (black) and the electroneutral NapA mutant K305A (red), in comparison with hNHA2 (green) and empty liposomes (blue).

antiport activity of a nonfunctional aspartate mutant is recoverable (Fig. 5*B*). Moreover, although D156N-K305Q was active, the D156N-K305N double mutant showed no activity. We speculate that the still polar, but slightly shorter, asparagine residue was not capable of restoring transport activity because the interaction between residues D156N and K305N is lost. It seems likely that D156 mutations might, therefore, be lethal because an unpaired lysine K305 results in highly unfavorable interactions, although more data are required to corroborate this.

Why is an interaction between D156 and K305 residues so important? As can been seen in NapA structures at physiological pH, the salt bridge between D156 and K305 is intact in the absence of a bound Na^+ ion (11, 16). This observation is in agreement with MD simulations of NhaA, in which the salt-bridge interaction needed to be broken to fully coordinate Na^+ (12). Our transport data show that, similarly to NhaA (14), the pH-dependent activity of NapA fits a kinetic model in which Na^+ and protons compete for the same ion binding site. As such, $Na^+(Li^+)$ binding and subsequent salt-bridge breakage should also catalyze proton release from K305. Consistent with this conventional antiport model (32), a recent MD study calculated that the pK_a of the equivalent lysine to K305 in NhaA (K300) is only lowered to a deprotonatable value once Na^+ binds (20). If, however, an uncharged residue replaces K305, the unpaired aspartate D156 will likely influence the efficiency of proton binding to D157. Our experiments using Li^+-driven antiport at different pH values support this hypothesis as, compared to WT, the polar electroneutral K305 variants became more active at lower pH values (Fig. 5*A*).

To explore the general requirement of a transmembrane embedded lysine for conferring electrogenicity in Na^+/H^+ antiporters, we analyzed the energetics of human NHA2, which is the only homologue where the two ion-binding aspartates are conserved, but the lysine residue equivalent to K305 has been replaced by arginine. Consistent with the electroneutral activity seen in the NapA variant K305R, we found that human NHA2 activity was likewise electroneutral. However, because human NHA2 shows higher ΔpH-driven antiport activity than equivalent electroneutral K305R variant in NapA (Table 1), clearly, the ion binding sites must be fine-tuned differently between these proteins. Indeed, we demonstrated via T126A and S127A activity measurements that transport kinetics in NapA is influenced by a variety of other residues in the vicinity of the ion binding site in addition to K305, D156, and D157. Such differences in the ion binding site environments could explain, for example, why the equivalent K300R variant in NhaA is much more active than that of K305R in NapA (10). A consequence of these differences could be that the salt bridge in NapA is stronger than in NhaA, and this may have evolved to ensure strict H^+ and Na^+ coupling at higher temperatures in *T. thermophilus* where NapA originates. Whatever the reason, clearly, structural and biochemical data will be required for each Na^+/H^+ antiporter to fully explain their mode of action. Along these lines, although we were successful in making NapA electroneutral, we have been unable to make NHA2 electrogenic by substituting R326 (equivalent to K305) with lysine or histidine as these mutants show poor antiport activity (Table 1). Such attempts have similarly failed to energize mammalian facilitative sugar porters, although converting bacterial proton-coupled sugar porters to be uniporters, through neutralization of a single charged residue, has been successful (33). We think the construction of such gain-of-function mutations will require a deeper understanding of the critical energetic barriers, which is clearly beyond the scope achievable here without further NHA2 structural and computational data.

Lastly, the importance of K305 likely extends beyond its role as a proton carrier and salt-bridge interaction partner to aspartate D156. The lysine K305 residue is also judicially positioned between the negatively charged dipoles of the discontinuous crossover helices in the core domain. Electron crystallography structures of homologous antiporters have shown that, upon Na^+ binding, the half-helices move substantially in the core domain (34–36). It is likely these core domain rearrangements are the

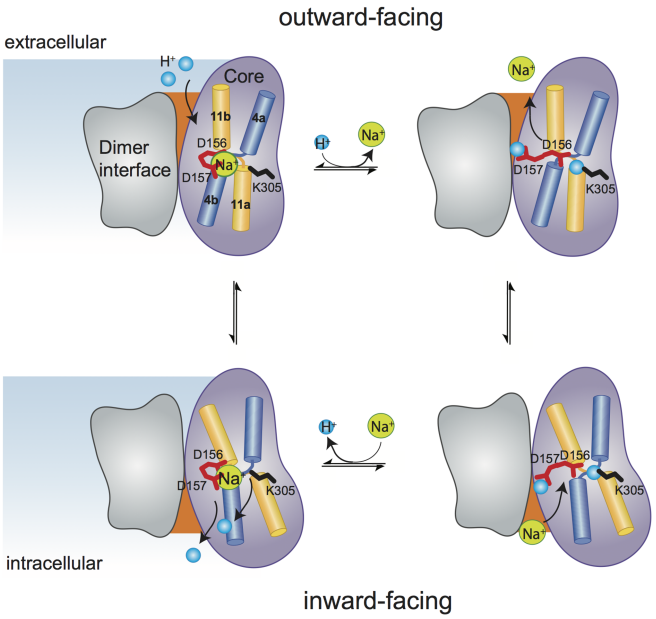

Fig. 7. Schematic of the NapA transport cycle. See last paragraph of *Discussion* for details.

prerequisite for facilitating the larger, elevator-like structural transitions seen in NapA crystal structures (11, 16), somewhat analogous to the core domain compaction intermediates seen upon substrate binding in other elevator proteins (33). Certainly, such an $Na^+(Li^+)$-sensitive salt bridge would be an elegant way to rapidly catalyze ion exchange with the conformational changes required for transport (34–36) (Fig. 7).

Taken together, our data challenges the prevailing assumption that the two ion-binding aspartates are the proton carriers in electrogenic Na^+/H^+ antiporters. This assumption was based on the fact that mutations of these residues results in an inactive transporter and that, in the electroneutral homologues, only one out of the two aspartates is conserved. Here, however, we have shown that (*i*) the lysine residue K305 is essential for electrogenic transport, (*ii*) activity of a nonfunctional D156N mutant can be rescued by the further mutation of lysine K305 to glutamine, and (*iii*) the activity of human NHA2, which harbors two aspartates, is nonetheless electroneutral, a suggestion that has previously been proposed from in vivo functional experiments (2, 37). We thus conclude that a transmembrane embedded lysine residue is a proton carrier and is essential for electrogenic Na^+/H^+ antiport.

Materials and Methods

Expression and Purification of Recombinant NapA and Human NHA2 Protein. NapA was cloned into pWaldo-GFPe with a C-terminal TEV-cleavable GFP-His_8 tag and overexpressed in the *E. coli* strain Lemo21 (DE3) as described previously (12). NapA and mutants were purified in the detergent DDM (Generon) by Ni-nitrilotriacetic acid (NTA) chromatography and size-exclusion chromatography as described previously. Human NHA2 (residues 70 to 480) was cloned into the GAL1 inducible TEV-cleavable GFP-His_8 2 μ vector pDDGFP2, transformed into the *S. cerevisiae* strain FGY217 (MATα, ura3–52, lys2Δ201, and pep4Δ), and overexpressed as described previously (27, 28). Human NHA2 was purified in DDM and cholesteryl hemisuccinae Tris salt (CHS) by Ni-NTA chromatography and size-exclusion chromatography, as described previously (27).

Na^+/H^+ Cysteine Accessibility (NapA V31C Mutant). Accessibility of cysteine residue was assessed by electrophoresis gel analysis following conjugation of methoxypolyethylene glycol maleimide (mPEG-5k; Sigma-Aldrich) to solvent-exposed cysteine thiol groups of the NapA mutant V31C. Five micrograms of purified NapA protein and 300 μL of liposomes, reconstituted with only NapA protein (see reconstitution protocol in *Coupled Proton Transport Assay Using ATP Synthase and NapA*, reconstitution without ATP synthase), were incubated with 5 mM mPEG-5k for 40 min at room temperature (RT). Liposomes were spun down for 30 min at 215,000 $\times$ *g*. Pellets were resuspended in the sample buffer. The resulting liposome samples with and without purified protein were analyzed by SDS/PAGE (NuPAGE Novex 4 to 12% Bis-Tris Protein Gels; Life Technologies).

Coupled Proton Transport Assay Using ATP Synthase and NapA. L-α-Phosphatidylcholine lipids from soybean (soybean lipids, type II, Sigma-Aldrich) were mixed with buffer consisting of 10 mM 3-(*N*-morpholino) propane sulfonic acid (Mops), pH 6.5, 5 mM $MgCl_2$, 100 mM KCl (MMK pH 6.5) to a final concentration of 10 mg/mL (w/v) and vortexed until homogenized. The lipids were flash-frozen in liquid nitrogen and then thawed, in a total of eight freeze–thaw cycles. Liposomes were subsequently extruded using polycarbonate filters (Whatman) with a pore size of 200 nm. For reconstitution experiments, 250 μL of liposomes were destabilized by addition of sodium cholate (0.65% final concentration) and mixed with 100 ug of NapA and *E. coli* F_0F_1 ATP synthase with an ~2:1 molar ratio (NapA:ATP synthase), and the suspension was incubated for 30 min at RT. Detergent was removed using a PD-10 desalting column, and the sample was collected in a final volume of 2.3 mL. Fifty microliters of NapA and ATPase containing proteoliposomes were diluted into 1.5 mL of reaction buffer (MMK buffer in the appropriate pH from 6 to 9) containing 2.5 nM ACMA and 130 nM valinomycin. An outward-directed pH gradient (acidic inside) was established by the addition of 130 μM ATP, as detected by a change in ACMA fluorescence at 480 nm using an excitation wavelength of 410 nm in a fluorescence spectrophotometer (Cary Eclipse; Agilent Technologies). After ~3 min equilibration, the activity of NapA WT and mutants thereof was assessed, after addition of the indicated concentrations of NaCl or LiCl, by a change in ACMA fluorescence. The addition of NH_4Cl, to a final concentration of 20 mM, dissipates the proton motive force and results in an almost complete dequenching using this experimental setup.

Functional Assays of NapA in Proteoliposomes Using Pyranine. ΔpLi or $\Delta\Psi$-driven proton H^+ transport, resulting from electrogenic Na^+/H^+ exchange activity, was monitored in liposomes using the highly soluble and membrane-impermeable pH-sensitive dye pyranine. An Na^+ or Li^+ gradient was established by the addition of NaCl or LiCl, whereas an electrical membrane potential was established with a K^+/valinomycin diffusion potential. Reconstitution of NapA into liposomes containing pyranine was essentially performed as described (11). In brief, a 500-μL liposome suspension (soybean lipids, type II, 20 mg/mL; Sigma-Aldrich) in buffer A (10 mM Mops-Tris, pH 8.0), 20 μL cholate [20% (w/v) stock solution] and 100 μg NapA purified as described previously was added, and the resulting samples were incubated for 30 min at RT. Cholate was removed via a PD-10 gel filtration column (GE Healthcare) equilibrated with buffer, with the reconstituted proteoliposomes collected in ~2.3 mL. The liposome sample was dialyzed overnight against buffer A at 4 °C for 16 h. The resulting dialysate was diluted to 8 mL by addition of buffer A, and the proteoliposomes were collected by ultracentrifugation (200,000 $\times$ *g*, 4 °C, 45 min) and resuspended in ~250 μL 2 mM Mops-Tris, pH 8.0. Subsequently, the proteoliposomes were mixed with 1 mM pyranine (0.1 M stock solution) and the desired Na_2SO_4 and K_2SO_4 concentrations (300 μL total volume of liposomes mixture). The resulting sample was twice frozen in liquid nitrogen, thawed in water, and briefly sonicated for 30 s. The nonincorporated pyranine was (subsequently) removed by size-exclusion chromatography using a G25 column (GE Healthcare) preequilibrated in buffer containing 2 mM Mops-Tris pH 8.0, 50 mM K_2SO_4, and either 0.5 or 50 mM Li_2SO_4. The proteoliposomes were collected from the first 1 mL of the eluate. Samples were diluted in 8 mL by addition of the equilibration buffer, concentrated by ultracentrifugation (200,000 $\times$ *g*, 4 °C, 45 min), and resuspended in 150 μL of the same buffer, containing the desired pH value. The pH change inside the proteoliposomes was monitored by fluorescence using the pyranine dye as described previously (11). In brief, 10 μL of the prepared proteoliposome solution was mixed with 2 mL of the desired measuring buffer, and the emission at 510 nm was recorded with alternating excitation wavelengths at 406 and 460 nm. For ΔpLi-driven experiments, liposomes containing 2 mM Mops-Tris, 0.5 mM Li_2SO_4, and 50 mM K_2SO_4 were mixed with 2 mL of the same buffer. Exchange activity was initiated after 20 s by the addition of 40 mM Li^+ to the outside. After 4 min, valinomycin (10 nM) was added to abolish an opposing membrane potential. For $\Delta\Psi$-driven experiments, 10 μL of liposomes containing 2 mM Mops-Tris, pH 8, 50 mM Li_2SO_4, and 50 mM K_2SO_4 were mixed with 2 mL of measuring buffer (2 mM Mops-Tris, pH 8, 50 mM Li_2SO_4,

and 0.25 mM K_2SO_4, i.e., no Li^+ gradient is present). Exchange activity was initiated after 20 s by addition of valinomycin (10 nM), establishing a membrane potential of −116 mV (inside negative) driving H^+ influx (and Li^+ efflux). Further potassium diffusion potentials were used to drive H^+ influx from 0 mV to −116 mV by modifying the outside-to-inside ratio of K_2SO_4 based on the Nernst equation. The ratio of pyranine 406 nm/460 nm (emission 510 nm) was converted into pH using a calibration curve, obtained using empty liposomes incubated at different pH values (see Fig. S1*E*). Proton influx and efflux were converted to ΔpH by subtraction of the pH (t = 0) from the measured pH upon initiation of transport activity.

Measurement of Membrane Potential Generation. The preparation of proteoliposomes for Li^+-driven antiport activity is identical to that described in *Functional Assays of NapA in Proteoliposomes Using Pyranine* except that ATP synthase was omitted during reconstitution. For measurements, 50 μL of proteoliposomes were mixed in a cuvette containing 1.5 mL of measuring buffer [50 mM Mops-Tris, pH 8.0, 10 mM K_2SO_4, 10 mM $(NH_4)_2SO_4$], 2.5 μM $DiSC_3(5)$ was added, and a baseline was recorded (excitation 651 nm; emission 675 nm). After 30 s, 50 mM LiCl was added and mixed rapidly. Finally, 130 nM valinomycin was added to abolish the membrane potential.

ACKNOWLEDGMENTS. This work was funded by grants from the Swedish Research Council (to D.D. and C.v.B.) and The Knut and Alice Wallenberg Foundation (to D.D. and C.v.B.). The authors are grateful for support to The Center for Biomembrane Research by the Swedish Foundation for Strategic Research. M.C. was a recipient of a Wenner-Gren postdoctoral fellowship, and D.D. acknowledges support from The European Molecular Biology Organization (EMBO) through the Young Investigator Program.

1. Padan E (2008) The enlightening encounter between structure and function in the NhaA Na^+–H^+ antiporter. *Trends Biochem Sci* 33(9):435–443.
2. Brett CL, Donowitz M, Rao R (2005) Evolutionary origins of eukaryotic sodium/proton exchangers. *Am J Physiol Cell Physiol* 288(2):C223–C239.
3. Taglicht D, Padan E, Schuldiner S (1993) Proton-sodium stoichiometry of NhaA, an electrogenic antiporter from *Escherichia coli*. *J Biol Chem* 268(8):5382–5387.
4. Pinner E, Padan E, Schuldiner S (1994) Kinetic properties of NhaB, a Na^+/H^+ antiporter from *Escherichia coli*. *J Biol Chem* 269(42):26274–26279.
5. Krulwich TA, Sachs G, Padan E (2011) Molecular aspects of bacterial pH sensing and homeostasis. *Nat Rev Microbiol* 9(5):330–343.
6. Hunte C, et al. (2005) Structure of a Na^+/H^+ antiporter and insights into mechanism of action and regulation by pH. *Nature* 435(7046):1197–1202.
7. Williams KA, Geldmacher-Kaufer U, Padan E, Schuldiner S, Kuhlbrandt W (1999) Projection structure of NhaA, a secondary transporter from *Escherichia coli*, at 4.0 A resolution. *EMBO J* 18(13):3558–3563.
8. Hu NJ, Iwata S, Cameron AD, Drew D (2011) Crystal structure of a bacterial homologue of the bile acid sodium symporter ASBT. *Nature* 478(7369):408–411.
9. Inoue H, Noumi T, Tsuchiya T, Kanazawa H (1995) Essential aspartic acid residues, Asp-133, Asp-163 and Asp-164, in the transmembrane helices of a Na^+/H^+ antiporter (NhaA) from *Escherichia coli*. *FEBS Lett* 363(3):264–268.
10. Maes M, Rimon A, Kozachkov-Magrisso L, Friedler A, Padan E (2012) Revealing the ligand binding site of NhaA Na^+/H^+ antiporter and its pH dependence. *J Biol Chem* 287(45):38150–38157.
11. Lee C, et al. (2013) A two-domain elevator mechanism for sodium/proton antiport. *Nature* 501(7468):573–577.
12. Lee C, et al. (2014) Crystal structure of the sodium-proton antiporter NhaA dimer and new mechanistic insights. *J Gen Physiol* 144(6):529–544.
13. Furrer EM, Ronchetti MF, Verrey F, Pos KM (2007) Functional characterization of a NapA Na(+)/H(+) antiporter from *Thermus thermophilus*. *FEBS Lett* 581(3):572–578.
14. Mager T, Rimon A, Padan E, Fendler K (2011) Transport mechanism and pH regulation of the Na^+/H^+ antiporter NhaA from *Escherichia coli*: An electrophysiological study. *J Biol Chem* 286(26):23570–23581.
15. Tzubery T, Rimon A, Padan E (2008) Structure-based functional study reveals multiple roles of transmembrane segment IX and loop VIII-IX in NhaA Na^+/H^+ antiporter of *Escherichia coli* at physiological pH. *J Biol Chem* 283(23):15975–15987.
16. Coincon M, et al. (2016) Crystal structures reveal the molecular basis of ion translocation in sodium/proton antiporters. *Nat Struct Mol Biol* 23(3):248–255.
17. Rosen BP (1986) Ion extrusion systems in *Escherichia coli*. *Methods Enzymol* 125:328–336.
18. Alkoby D, et al. (2014) NhaA Na^+/H^+ antiporter mutants that hardly react to the membrane potential. *PLoS One* 9(4):e93200.
19. Zuber D, et al. (2005) Kinetics of charge translocation in the passive downhill uptake mode of the Na^+/H^+ antiporter NhaA of *Escherichia coli*. *Biochim Biophys Acta* 1709(3):240–250.
20. Huang Y, Chen W, Dotson DL, Beckstein O, Shen J (2016) Mechanism of pH-dependent activation of the sodium-proton antiporter NhaA. *Nat Commun* 7:12940.
21. Fuster DG, Alexander RT (2014) Traditional and emerging roles for the SLC9 Na^+/H^+ exchangers. *Pflugers Arch* 466(1):61–76.
22. Xiang M, Feng M, Muend S, Rao R (2007) A human Na^+/H^+ antiporter sharing evolutionary origins with bacterial NhaA may be a candidate gene for essential hypertension. *Proc Natl Acad Sci USA* 104(47):18677–18681.
23. Fuster DG, et al. (2008) Characterization of the sodium/hydrogen exchanger NHA2. *J Am Soc Nephrol* 19(8):1547–1556.
24. Kondapalli KC, Kallay LM, Muszelik M, Rao R (2012) Unconventional chemiosmotic coupling of NHA2, a mammalian Na^+/H^+ antiporter, to a plasma membrane H^+ gradient. *J Biol Chem* 287(43):36239–36250.
25. Deisl C, et al. (2013) Sodium/hydrogen exchanger NHA2 is critical for insulin secretion in β-cells. *Proc Natl Acad Sci USA* 110(24):10004–10009.
26. Chintapalli VR, et al. (2015) Transport proteins NHA1 and NHA2 are essential for survival, but have distinct transport modalities. *Proc Natl Acad Sci USA* 112(37):11720–11725.
27. Drew D, et al. (2008) GFP-based optimization scheme for the overexpression and purification of eukaryotic membrane proteins in Saccharomyces cerevisiae. *Nat Protoc* 3(5):784–798.
28. Newstead S, Kim H, von Heijne G, Iwata S, Drew D (2007) High-throughput fluorescent-based optimization of eukaryotic membrane protein overexpression and purification in *Saccharomyces cerevisiae*. *Proc Natl Acad Sci USA* 104(35):13936–13941.
29. Padan E, et al. (2004) NhaA of *Escherichia coli*, as a model of a pH-regulated Na^+/H^+antiporter. *Biochim Biophys Acta* 1658(1-2):2–13.
30. Wohlert D, Kuhlbrandt W, Yildiz O (2014) Structure and substrate ion binding in the sodium/proton antiporter PaNhaP. *Elife* 3:e03579.
31. Zhou X, et al. (2014) Structural basis of the alternating-access mechanism in a bile acid transporter. *Nature* 505(7484):569–573.
32. Schuldiner S (2014) Competition as a way of life for H(+)-coupled antiporters. *J Mol Biol* 426(14):2539–2546.
33. Drew D, Boudker O (2016) Shared molecular mechanisms of membrane transporters. *Annu Rev Biochem* 85(1):543–572.
34. Vinothkumar KR, Smits SH, Kuhlbrandt W (2005) pH-induced structural change in a sodium/proton antiporter from *Methanococcus jannaschii*. *EMBO J* 24(15):2720–2729.
35. Appel M, Hizlan D, Vinothkumar KR, Ziegler C, Kuhlbrandt W (2009) Conformations of NhaA, the Na^+/H^+ exchanger from *Escherichia coli*, in the pH-activated and ion-translocating states. *J Mol Biol* 388(3):659–672.
36. Paulino C, Kuhlbrandt W (2014) pH- and sodium-induced changes in a sodium/proton antiporter. *Elife* 3:e01412.
37. Taglicht D, Padan E, Schuldiner S (1991) Overproduction and purification of a functional Na^+/H^+ antiporter coded by NhaA (ant) from *Escherichia coli*. *J Biol Chem* 266(17):11289–11294.